DETERMINATION OF PERSISTENCE EFFECTS IN SPATIO-TEMPORAL PATTERNS OF UPWARD LONG-WAVE RADIATION FLUX DENSITY FROM AN URBAN COURTYARD BY MEANS OF TIME-SEQUENTIAL THERMOGRAPHY

Fred Meier[1]*, Dieter Scherer*, Jochen Richters*
*Chair of Climatology, Department of Ecology, Technische Universität Berlin, Germany

Abstract
This research analyses upward long-wave radiation flux density from urban surfaces using a high-resolution thermal-infrared (TIR) camera and meteorological measurements in the city of Berlin, Germany. We report spatio-temporal patterns of the difference between upward long-wave radiation flux density from courtyard surfaces and the roof. Thermal patterns show persistence effects due to shadow, sky view factor (SVF) distribution, thermal properties of surface materials, human activities and turbulence characteristics of the surface-atmosphere interface. The attenuation of thermal patterns caused by temporary disturbances due to parked cars can be described by a modified exponential curve and a time-constant. This study shows that ground-based high-resolution TIR imagery is highly suitable to investigate dynamic processes controlling thermal patterns within a complex three-dimensional urban structure.

Key words: time-sequential thermography, thermal persistence, shadow

1. INTRODUCTION

Ground-based remote sensing using thermal-infrared (TIR) camera systems mounted on masts, towers or building roofs provide an alternative to airborne and satellite platforms for acquisition of spatially distributed TIR data at both high spatial and high temporal resolution. Voogt & Oke (2003) expect progress in urban climate research due to availability and application of low-cost, high-resolution portable TIR scanner systems. In Tokyo, a TIR camera system continuously measured urban surface temperatures for derivation of a town-scale thermal property parameter (Sugawara et al. 2001). At the building scale, Hoyano et al. (1999) used time-sequential thermography (TST) for calculating sensible heat flux density. Thermal characteristics of various urban surfaces in Tel-Aviv were assessed by using a thermal video radiometer that captured images from a high-rise building (Chudnovsky et al. 2004).
The three-dimensional city structure generates a complex pattern of partially sunlit and shadowed surfaces in particular under cloudless conditions. Depending on shadow, different surfaces receive different short-wave irradiance. In a more general perspective, a thermal persistence effect is activated by a specific disturbance in the surface-atmosphere system. A question is how long is this disturbance detectable in the system? The high-spatial resolution infrared image simulator OSIrIS reproduces the persistence of shadow effects in complex urban environments (Poglio et al. 2006). Persistence in this paper stands for a temporal stability of spatial patterns of upward long-wave radiation flux density. This study addresses following two questions.

1.) How important is the history of shadow for upward long-wave radiation flux density from courtyard surfaces?
2.) Can we observe different persistence effects in spatio-temporal patterns of upward long-wave radiation flux density?

In order to answer these questions we observe and analyse spatio-temporal variability of upward long-wave radiation flux density using an oblique viewing high-resolution TIR camera system capturing images at scales in the range of centimeters. The TIR imaging system operates in a spectral window between 7.5 µm and 14 µm and consist of micro-bolometer measurement device with a focal plane array (320 x 240 pixels). We can expect strong surface temperature variations due to emissivity differences at this micro-scale (Voogt & Oke 1997). Measurements of emissivity for all surfaces in the field of view (FOV) are beyond the scope of this project. Therefore, the focus is on upward long-wave radiation.

2. METHODOLOGY

2.1 Experimental setup

The study site is located in Berlin (Germany) in the Charlottenburg-Wilmersdorf district close to the city centre Zoologischer Garten. City structure is characterized by five to six-story perimeter block development. This micro-scale TIR remote sensing study was part of a local-scale urban climatology experiment including boundary layer

[1] Corresponding author: Fred Meier, Chair of Climatology, Department of Ecology, Technische Universität Berlin, Rothenburgstr. 12, D-12165 Berlin, Germany, E-mail: fred.meier@tu-berlin.de

meteorological measurements such as directly measured sensible heat flux density, air temperature and humidity. We call it Stilwerk Experiment according to the name of the shopping mall, whose roof provided a basis for measurement installations. The TIR camera was oriented towards North (354°) and inclined by 20° from the nadir angle. In the courtyard FOV the essential features are one lime tree, a narrow green terrace (9.4 m above courtyard floor), an asphalt loading zone and a paved car-park. The TIR camera recorded one image per minute over a period of 48 hours from 3rd to 5th May 2007. The fixed camera position ensures a valid comparison between the multi-temporal imagery. Two meters above the building roof all four components of the radiation balance (Kipp & Zonen, CNR1) were recorded at one minute intervals.

2.2 Pre-processing, radiometric and geometric corrections of TIR imagery

The first step of image processing uses firmware calibration parameters for converting measured radiance into directional brightness temperatures (Tb) for each pixel. This assumes that the detected surface is a Lambertian blackbody. In order to avoid drift effects these internal image calibration has to be done in the same interval, or at higher frequency, than the measurement interval. If the system operates with an internal calibration frequency lower than the measurement interval then minor artificial jumps from one image acquisition to the next are possible due to changes in case temperature. Lens effects disturb TIR data. Experiments showed a clear 1.2 K difference of Tb from the centre of the TIR image to the corners. This lens effect was corrected by using a data set of dense fog and assuming isotropic distribution of radiance (Christen et al. 2006). Other experiments (Lagouarde et al. 2004) also reported such effects. In addition, geometric lens deformations have been analysed in our laboratory by measuring a grid of metallic pins in a regular square pattern. After geometric correction the TIR image covers a FOV of 57.5° by 44.7°. Due to short target-sensor distances no atmospheric correction procedure was applied. Finally, Tb was reconverted into long-wave radiation flux density via Stefan-Boltzmann law:

$$E_{TST}(\vec{x}_i,t) = \sigma T_b{}^4(\vec{x}_i,t) \qquad (1),$$

where $\vec{x}_i$ represents each pixel and its spatial position in the courtyard, t is the acquisition time of the TIR image. The resultant imagery $E_{TST}(\vec{x}_i,t)$ consists of 2880 TIR images that can be considered as a spatio-temporal image-cube.

2.3 Determination of persistence effects

Analysis of persistence effects is based upon the difference $\Delta E_{ref}(\vec{x}_i,t)$ between upward long-wave radiation from a shadowed (disturbed) surface and a non-shadowed (undisturbed) reference surface. Simply because the roof is always non-shadowed and in order to determine persistence effects in relation to the daily cycle, we selected the roof as a reference surface. It is possible to select another undisturbed reference surface e. g. in order to analyze short-term persistence effects or surface material properties. The spatio-temporal patterns of mean difference (MD) as well as standard deviation of difference (SDD) and mean rate of change of difference (MROCD) between upward long-wave radiation from courtyard surfaces (TIR imagery) and upward long-wave radiation from building roof (CNR1 pyrgeometer) provide the basis for persistence analysis. There are some assumptions underlying this approach. At first, we disregard the spectral range discrepancy. The CNR1 pyrgeometer is a broadband (3 µm to 100 µm) and the TIR camera is a narrowband measurement device. Secondly, we have to consider that measured upward long-wave radiation include reflections from downward long-wave radiation because surface emissivity values are less than unity.

3. RESULTS AND DISCUSSION

During the investigation period, clear sky conditions caused high downward short-wave irradiance with a maximum of 850 Wm^{-2} around noon. These atmospheric conditions allow for detailed analysis of the diurnal variation in upward long-wave radiation.

3.1. Daily mean patterns

Modifying the contrast can enhance the ability to extract pattern information from the image. Hence, we scaled calculated patterns (Fig. 1) between the 95% percentile (red) and the 5% percentile (blue). All color bars have benchmarks for the median (50%), the minimum, maximum and zero value of the computed mean pattern. In addition, the MD pattern shows areas of interest (AOI), see also Table 1 for AOI description. The daily MD median is negative (-25.5 Wm^{-2}). The sunlit treetop has a slight higher MD (-22.9 Wm^{-2}) in comparison to the temporarily shadowed treetop (-24.9 Wm^{-2}). Even the car-park area between the parked cars and therefore situated in the car shadow has negative MD values. Only the cars and the car-park area covered by concrete paving stones show positive MD values in spite of afternoon tree shadow. The whole car-park shows a slight gradient from the eastern to the western part (Fig. 1 left). This thermal gradient is a persistence effect resulting from the history of shadow. The daily SDD median (55 Wm^{-2}) is higher than the daily MD median (Fig. 1, middle). This results from the accumulation of day and night differences between the courtyard and the roof. For instance, the asphalt loading

zone and the wall show the highest SDD values as a consequence of completely different conditions during the day (shadow) and during the night (lower SVF) in comparison to the roof. The car surfaces show also high SDD values. This is a consequence of car movement and thermal performance of metallic surfaces.

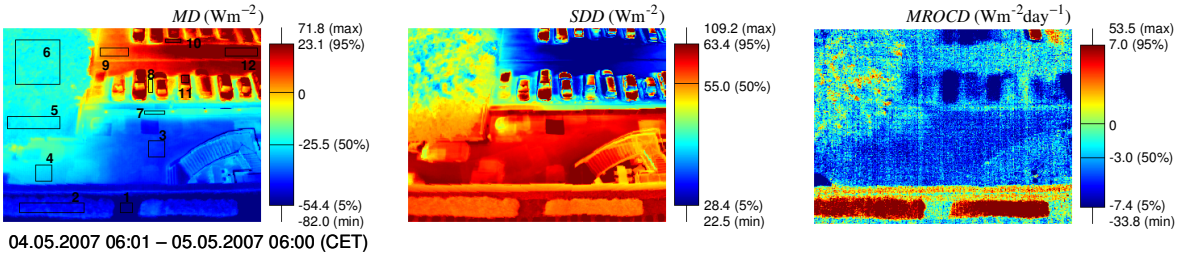

Figure 1: Spatio-temporal patterns of mean difference (MD) (left), standard deviation of difference (SDD) (middle) and mean rate of change of difference (MROCD) between upward long-wave radiation from courtyard surfaces and upward long-wave radiation from building roof for a 24-hourly cycle. The MD pattern shows areas of interest (AOI), see also Table 1.

The original 24-hourly MROCD values at one minute resolution were multiplied by 1440 to represent changes at the daily scale. Therefore, this pattern comprises spatial information about alteration in upward long-wave radiation between 06:01 and 06:00 next morning in relation to the roof. This pattern is completely different in comparison to the 24-hourly MD and SDD patterns. It is not possible to identify features, which correspond to thermal gradients like the car-park area shown in the 24-hourly MD pattern or to the dichotomy in terms of northern sunlit and southern shadowed part. On closer examination, this 24-hourly MROCD pattern shows lower values for the asphalt loading zone than for the car-park area. Furthermore, shadow due to parked cars produced the lowest MROCD values. In general, we measured a slight decrease of upward long-wave radiation flux density for artificial courtyard surfaces in this 24-hourly period. Only the hedgerow on the terrace has positive MROCD values. The biomass of the vegetation is not able to store or conduct heat into ground in the same way as artificial surfaces. Air temperature is very important for modulation of vegetation surface temperature and upward long-wave radiation respectively. The measured air temperatures can be used to explain MROCD pattern for the hedgerow. During the experiment we measured air temperature (Campbell CS 215) 1.3 m above the terrace and very close to the hedgerow. For this 24-hourly period we recorded an increase in air temperature of 1 K. This might be the reason for the positive MROCD values. Interestingly some branches show higher MROCD values than the rest of the treetop. These parts are probably more influenced by turbulence processes.

Table 1: Spatio-temporal average of mean difference (MD), standard deviation of difference (SDD) and mean rate of change of difference (MROCD) for selected areas of interests (AOI) from 4th May 06:01 to 5th May 06:00 Central European Times (CET), see also Fig. 1 (left) for AOI positions.

	AOI description (AOI pixel size)	MD (Wm^{-2})	SDD (Wm^{-2})	MROCD ($Wm^{-2}day^{-1}$)
1	Terrace gravel (16 x 13)	-62.0	61.8	-0.7
2	Terrace hedgerow (81 x 13)	-43.9	56.3	+8.1
3	Asphalt loading zone, central (21 x 21	-41.3	60.6	-5.2
4	Asphalt loading zone, left(21 x 21)	-28.1	62.6	-4.3
5	Treetop, shadowed (66 x 16)	-24.9	53.7	-1.9
6	Treetop, sunlit (66 x 66)	-22.9	46.1	-1.4
7	Wall (26 x 5)	-24.3	61.9	-4.9
8	Honeycomb-type paving stones with grass (6 x 17)	-7.1	34.2	-4.5
9	Concrete paving stones, West (36 x 11)	+5.5	36.0	-3.5
10	Honeycomb-type paving stones with grass (20 x 5)	+21.0	25.5	-4.0
11	Car (10 x10)	+22.2	52.3	-9.9
12	Concrete paving stones, East (41 x 11)	+28.0	31.4	-2.0

3.2. Attenuation of temporary disturbances

The attenuation of upward long-wave radiation differences caused by temporary disturbances due to parked cars was further analysed. The difference $\Delta E_{ref}(t)$ between temporary shadowed and non-shadowed surfaces inside the courtyard is defined as:

$$\Delta E_{ref}(t) = \left\langle E_{TST}(\vec{x}_{shd}, t)\right\rangle - \left\langle E_{TST}(\vec{x}_{ref}, t)\right\rangle, \qquad (2)$$

where $\left\langle E_{TST}(\vec{x}_{shd}, t)\right\rangle$ is the spatial mean of the previous shadowed parking space and $\left\langle E_{TST}(\vec{x}_{ref}, t)\right\rangle$ is the spatial mean of neighboring previous non-shadowed reference surface (same material). The decrease of $\Delta E_{ref}(t)$ in the course of time can be described by:

$$\Delta E_{ref}(t - t_0) = \Delta E_{ref}(t_0)\exp\left(-\sqrt{\frac{t - t_0}{\tau}}\right), \qquad (3)$$

where $\Delta E_{ref}(t-t_0)$ is the difference of upward long-wave radiation flux density in the course of time after car departure and $\Delta E_{ref}(t_0)$ is the difference immediately after car departure. The time-constant τ is defined as:

$$\frac{\Delta E_{ref}(\tau)}{\Delta E_{ref}(t_0)} = \exp(-1)\ . \qquad (4)$$

In the TIR imagery dataset, we found several of these temporary persistence effects. The following graphs in Fig. 2 show the good agreement between calculated values from Eq. 3 and measured TIR data. In addition, secondary disturbances can influence the equalization process. If one secondary disturbance (e.g. due to tree shadow) appears at the beginning of the equalization process than a clear deceleration (Fig. 2 left, secondary disturbance at first present at previous shadowed surface) or acceleration (Fig. 2 middle, secondary disturbance at first present at reference surface) of the process becomes apparent.

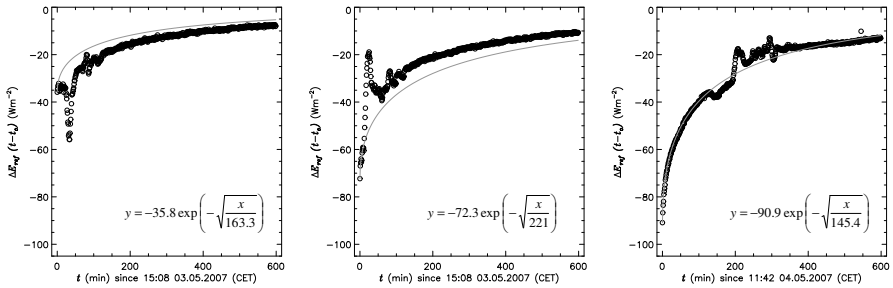

Figure 2: Equalization of the upward long-wave radiation difference between the temporary shadowed car-park surfaces and the reference surfaces close to it. Decay curves derived from exponential equations noted below, based on Eq. 3. Surface materials: honeycomb paving stones with grass (left, middle) and concrete paving stones (right).

4. CONCLUSIONS AND OUTLOOK

We can conclude that the history of shadow i.e. when shadow is present on the surface is important for the daily MD pattern. The daily MROCD pattern depends on shadow duration i.e. how long shadow has been present on the surface and on air temperature changes. The thermal patterns show persistence effects because of shadow, SVF distribution, human activities and turbulence characteristics of the surface-atmosphere interface. In order to prove the assumed SVF distribution in the courtyard and to make spatial correlations with thermal patterns it is possible to apply urban digital elevation models. Further studies will address the derivation of surface thermal properties and the role of solar irradiation as well as atmospheric turbulence during the equalization of persistence effects.

References

Christen, A., Scherer, D., Mielke, M., 2006. High frequency patterns in urban surface temperatures. *EARSeL – First Workshop of the Special Interest Group on Urban Remote Sensing*, March 2-3 2006, Berlin, Germany.

Chudnovsky, A., Ben-Dor, E., Saaroni, H., 2004. Diurnal thermal behavior of selected urban objects using remote sensing measurements. *Energy and Buildings*, 36, 1063-1074.

Hoyano, A., Asano, K., Kanamaru, T., 1999. Analysis of the sensible heat flux from the exterior surface of buildings using time sequential thermography. *Atmospheric Environment*, 33, 3941-3951.

Lagouarde, J. P., Moreau, P., Irvine, M., Bonnefond, J. M., Voogt, J. A., Solliec, F., 2004. Airborne experimental measurements of the angular variations in surface temperature over urban areas: case study of Marseille (France). *Remote Sensing of Environment*, 93, 443-462.

Poglio, T., Mathieu-Marni, S., Ranchin, T., Savania, E., Wald, L., 2006. OSIrIS: a physically based simulation tool to improve training in thermal infrared remote sensing over urban areas at high spatial resolution. *Remote Sensing of Environment*, 104, 238-246.

Sugawara, H., Narita, K., Mikami, T., 2001. Estimation of effective thermal property parameter on a heterogeneous urban surface. *Journal of the Meteorological Society of Japan*, 79, 1169-1181.

Voogt, J. A., Oke, T. R., 1997. Complete urban surface temperatures. *Journal of Applied Meteorology*, 36, 1117-1132.

Voogt, J. A., Oke, T. R., 2003. Thermal remote sensing of urban climates. *Remote Sensing of Environment*, 86, 370-384.